

Structural behaviour of high strength steel hexagonal hollow section stub columns under axial compression

Jun-zhi Liu¹; Han Fang³; Tak-Ming Chan^{1,2 *}

¹ Department of Civil and Environmental Engineering, The Hong Kong Polytechnic University, Hong Kong, China

² Chinese National Engineering Research Centre for Steel Construction (Hong Kong Branch), The Hong Kong Polytechnic University, Hong Kong, China

³ School of Civil Engineering, University of Leeds, United Kingdom (formerly, School of Civil, Environmental and Mining Engineering, The University of Adelaide, South Australia 5005, Australia)

* Corresponding author: tak-ming.chan@polyu.edu.hk

Abstract

This paper presents a comprehensive experimental investigation into the structural behaviour of the high strength steel (HSS) hexagonal hollow sections (HexHS) stub columns under concentric compression. A total of 18 HSS HexHS stub columns encompassing three fabrication routes were performed. The HSS plates used to fabricate the specimen were delivered in Quenched and Tempered (QT) condition. The Material properties within the cross sections of the HSS HexHS were measured. Initial local geometric imperfections for all the examined stub columns were measured. The cross-section slenderness yield limits in the existing design codes of the EN 1993-1-12, ANSI/AISC 360-16, AS 4100 and ASCE/SEI 48-11 were compared and assessed against the experimental results. It was found that the current limits for internal compression plates in HSS rectangular and square sections cannot be extended to cover the cross-section classification for HSS HexHS. In terms of the cross-sectional resistance predictions, all the design codes tend to under-estimate the resistance of HSS HexHS under axial compression. For sections failed by local buckling prior to the attainment of yield load, the AS 4100 yields more accurate predictions compared with those predictions based on the other design codes. Compared with the design approach of Direct Strength Method (DSM), Continuous Strength Method (CSM) provides more consistent and satisfactorily predictions, particularly for stocky sections due to the consideration of strain hardening.

Keywords: Local buckling behaviour; Hexagonal hollow sections; High strength steel; Axial compression;

27 Experiments; Design methods.

28 **1. Introduction**

29 Steel tubular hollow sections are widely adopted in the construction industry such as buildings, bridges and
30 offshore structures because of the aesthetic appearance and high resistance against local or torsional buckling
31 [1–3]. The family of tubular hollow sections typically comprises conventional rectangular (RHS), square (SHS)
32 and circular hollow sections (CHS). The advanced manufacturing technology allows the formation of tubular
33 hollow sections in different cross-section configurations with combined structural efficiency and architectural
34 aesthetics. With these considerations, elliptical hollow sections (EHS) are available in the market and their
35 structural performance under various loading conditions have been studied by Chan and Gardner [4–6].
36 Besides, cold-formed steel oval hollow sections have also been investigated by Zhu and Young [7] and cold-
37 formed semi-oval hollow sections have been studied by Chen and Young [8–9]. Recently, octagonal hollow
38 sections (OctHS) at material level and cross-section level have been investigated in Fang et al. [2] and Liu et
39 al. [10, 11] comprising Q690 steel plates with nominal yield strength of 690 MPa, and Q460 steel plates with
40 nominal yield strength of 460 MPa in Chen et al. [12–13] and Q355 steel plates with nominal yield strength of
41 355 MPa in Zhu et al. [14]. The applicability of the existing design rules and design approaches have been
42 assessed.

43 Apart from the aforementioned tubular sections, in recent years, hexagonal hollow sections (HexHS) have also
44 attracted increasing interests from structural engineers and architects [15–16]. An illustrative advantage of
45 HexHS is that the width of the flat portion is smaller than square and rectangular counterparts if they are
46 delivered with similar perimeters, therefore exhibiting stronger local buckling resistance than that of square
47 and rectangular hollow sections (SHS and RHS). In addition, the flat surfaces allow for easier construction by
48 providing an operating platform for welding- or bolt-connection with end plate or gusset plate. Despite the
49 potential advantages of HexHS in structural application, limited investigations on their structural performance

50 have been conducted.

51 Previous research studies for hexagonal tubular section structural members primarily focused on those

52 fabricated with conventional strength steel materials. Aoki et al. [17] conducted stub column tests on hexagonal

53 tubular sections formed by welding six steel plates, as shown in Fig. 1(a). Mitiga et al. [18] carried out

54 investigation on the structural behaviour of hexagonal hollow sections formed by welding two half-sections

55 with two cold-bent corners for each half-section, as shown in Fig. 1(b). Godat et al. [19] performed stub column

56 tests to investigate the local buckling behaviour of hexagonal sections formed by welding two half sections.

57 Each half section was produced by press-braking with three cold-bent corners, as depicted in Fig. 1(c). In the

58 study, a design method based on test results was also proposed for predicting the capacity of the stub columns.

59 For high strength steel (HSS) hexagonal hollow sections (HexHS) and irregular hexagonal hollow sections

60 (IHexHS), research was mainly conducted to investigate the material properties [15–16], and structural

61 performance at cross-sectional level was studied in [20]. However, no research investigation has been carried

62 out to study the local buckling behaviour of the high strength steel HSS HexHS. Hitherto, design rules

63 concerning cross-section classification and cross-section strength for HexHS is specified in ASCE/SEI 48-11

64 [[21]. However, design guidelines for HexHS are not included in any structural steel design specification like

65 the Eurocode of EN 1993-1-12 [22], EN 1993-1-5 [34], North American code of ANSI/AISC 360-16 [23], and

66 Australian code of AS 4100 [24]. The applicability of these design rules to HSS HexHS needs to be evaluated.

67 To have a safe and economical design for HSS HexHS, this paper therefore presents an experimental

68 investigation on the cross-sectional behaviour of HSS hexagonal tubular sections encompassing three different

69 fabrication routes under axial compression. The material properties for each cross-section series were

70 measured by extracting the coupons from the flat portion and corner portion of the sections. The initial local

71 geometric imperfections of each cross-section series were also measured. After completion of the stub column

72 tests, the obtained test results were used to compare with design strengths predicted by current design methods.

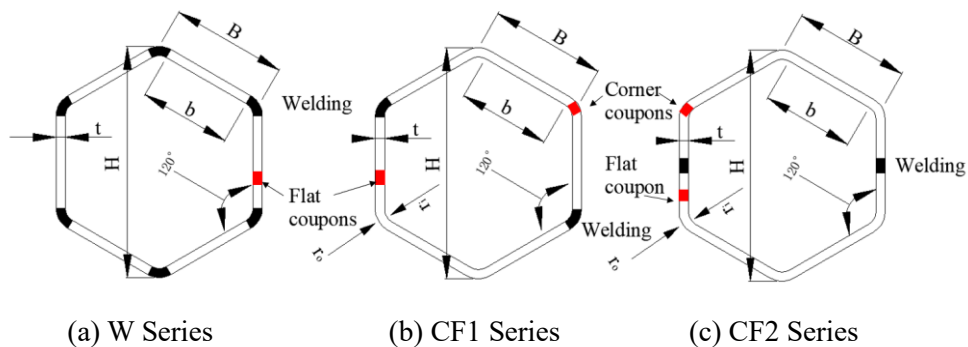
73

74

75 2. Test specimens

76 2.1 General

77 Three series of HSS HexHS were included in the experimental programme with the cross-section geometry as
78 defined using the symbols in Fig. 1, where H is the height of the cross section, B is the edge width of the
79 HexHS, b is the clear width of a flat side excluding the corner portions and the welding bead, t is the thickness
80 of the cross section, r_o and r_i are the outer corner radius and inner corner radius of the cross section, respectively.
81 Each series of the HSS HexHS corresponds to one fabrication route. The first “W” series indicates the built-
82 up HSS HexHS fabricated by welding six HSS plates. The second series of HSS HexHS were fabricated by
83 welding two-half sections with each half-section featured with two cold-bent corners and the welding seam
84 was located at the two corners, denoted as “CF-1”. The third series of HSS HexHSs were fabricated by welding
85 two half-sections, and each half-section has three cold-bent corners with welding operated at flat portion,
86 denoted as series “CF-2”. HSS plates with nominal thicknesses of 6 mm and 10 mm and the grade of Q690
87 were used to fabricate the HSS HexHS in this study.



88

89

90

91

Fig. 1. Cross sectional views of the examined HSS HexHS stub column specimens [15].

92

93

A total of 18 HSS HexHS stub columns were examined in the experimental tests. The specimen label system including detailed information about the nominal cross section geometry was used in this paper. Following the

cross-sectional shape of the specimen, the nominal dimensions ($B \times t$) of the HSS HexHS was denoted with fabrication route given after hyphen, the symbol of “#” was used to indicate the repeated tests. For example, the specimen of “HEX-155 \times 10-W#” indicates that a repeated specimen which was fabricated by the first fabrication route with a nominal edge width B of 155 mm and nominal thickness of 10 mm. The detailed definition of the symbols within the cross section are demonstrated in Fig. 2.

Table 1 Mean test results of the flat coupons taken from the HSS parent plates [15].

Section	$E_{s,p}$ (GPa)	ν	$f_{y,p}$ (Mpa)	$f_{u,p}$ (Mpa)	$\epsilon_{u,p}$ (%)	$\epsilon_{t,p}$ (%)	$\epsilon_{sh,p}$ (%)
6 mm plate	214.1	0.29	768.5	816.2	6.45	14.95	1.98
10 mm plate	216.1	0.30	791.3	825.6	6.55	16.18	2.32

In particular, the thickness measurements were conducted along the column length using ultrasonic measuring gauge as shown in Fig. 3 and the digital Vernier caliper was used to measure the thickness at the end section, with the mean values of the thickness reported in Table 1. The edge width of B ranges from 71.6 mm to 206.9 mm and the measured thickness varies between 5.89 mm to 9.81 mm, resulting in a ratio of side width to thickness b/t ranging from 7.6 to 31.9.

2.2 Material properties measurements

Material properties were firstly determined by conducting tensile coupon tests. Detailed testing procedure, including the loading strain rate, designated coupon dimensions, coupon failure modes, and the experimental observations were fully reported in [15]. Key information is summarised herein. Three longitudinal and three transverse tensile coupons were taken from each parent plate with thickness of 6 mm and 10 mm respectively, resulting in a total of 12 parent tensile coupons. The tensile coupon specimens were extracted within the cross-sections of the HSS HexHS from two critical locations, namely the flat and the corner portions. The dimensions of the tensile coupon specimens were designed in accordance with ISO EN 6892-1: 2019 [25]. For testing the specimens, an in-house electromechanical high force universal testing system of Instron 5982 testing machine with a capacity of 100 kN was used. The test arrangement for the flat- and corner tensile coupons is presented

119 in Fig. 4.

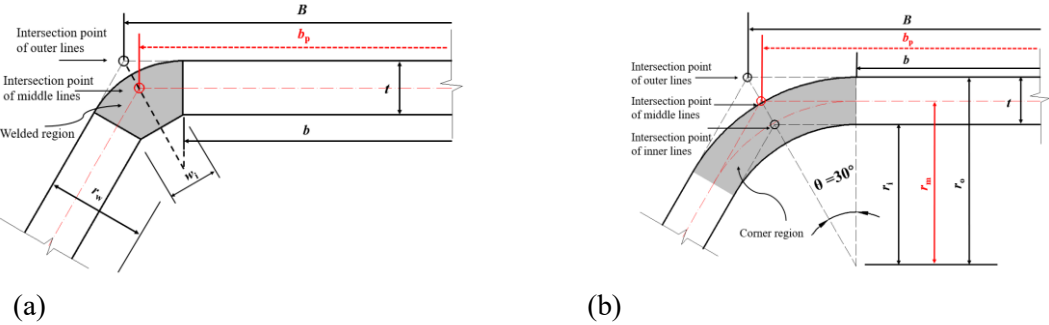


Fig. 2. Detailed geometries and definitions of the symbols for HSS hexagonal hollow sections (a) W-series (b) CF1-series and CF2-series.

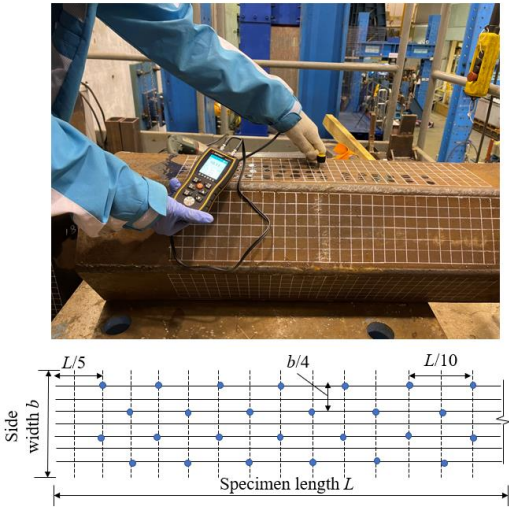


Fig. 3. Thickness measurement for HSS hexagonal hollow sections using ultrasonic measuring gauge.

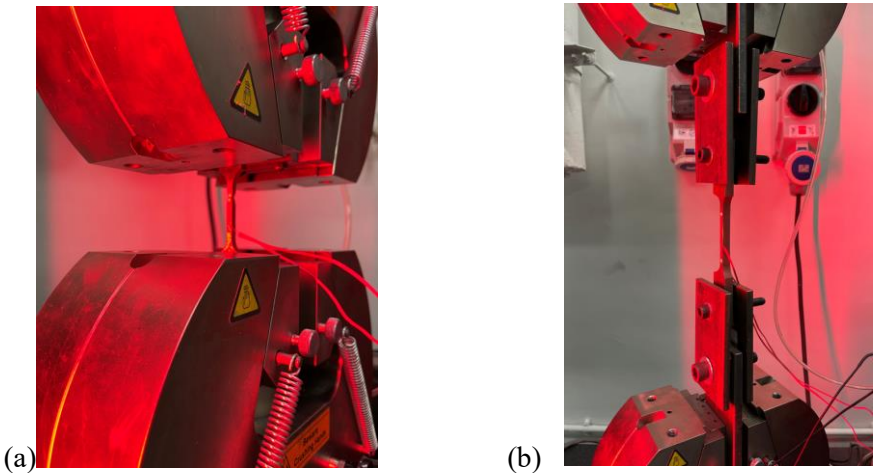


Fig. 4. Test arrangements of the tensile coupon specimens (a) Flat and parent coupons (b) Corner coupons

For testing the specimens extracted from the corner regions, two holes with diameter of 10 mm were drilled at

the distance of 20 mm from the end of the corner coupon. A pair of specially developed grips with two pins was utilised to apply the tensile load through its centroid, as seen in Fig. 4(b). Fig. 5 shows the measured stress-strain relationships for the parent tensile coupons taken from the steel plate longitudinally and transversely with the key average measured material properties including the elastic modulus E_s , the yield strength f_y , the ultimate strength f_u , hardening strain ε_{sh} , strain at ultimate strength ε_u , and elongation at fracture ε_f reported in Table 1.

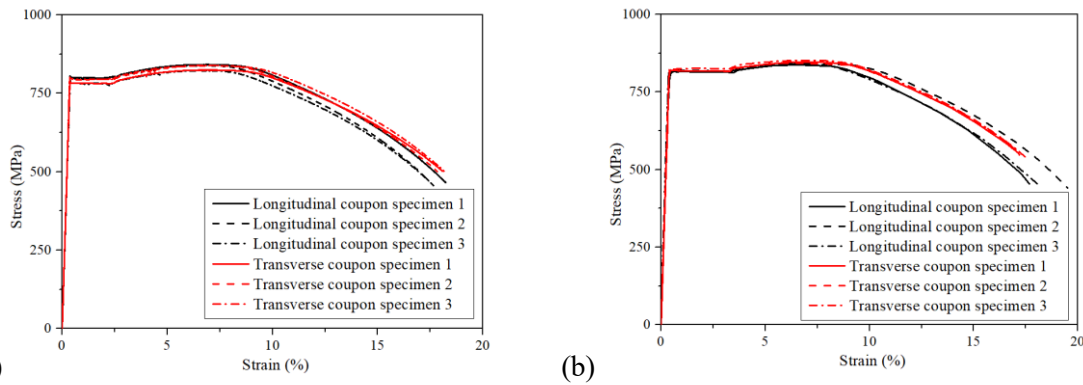
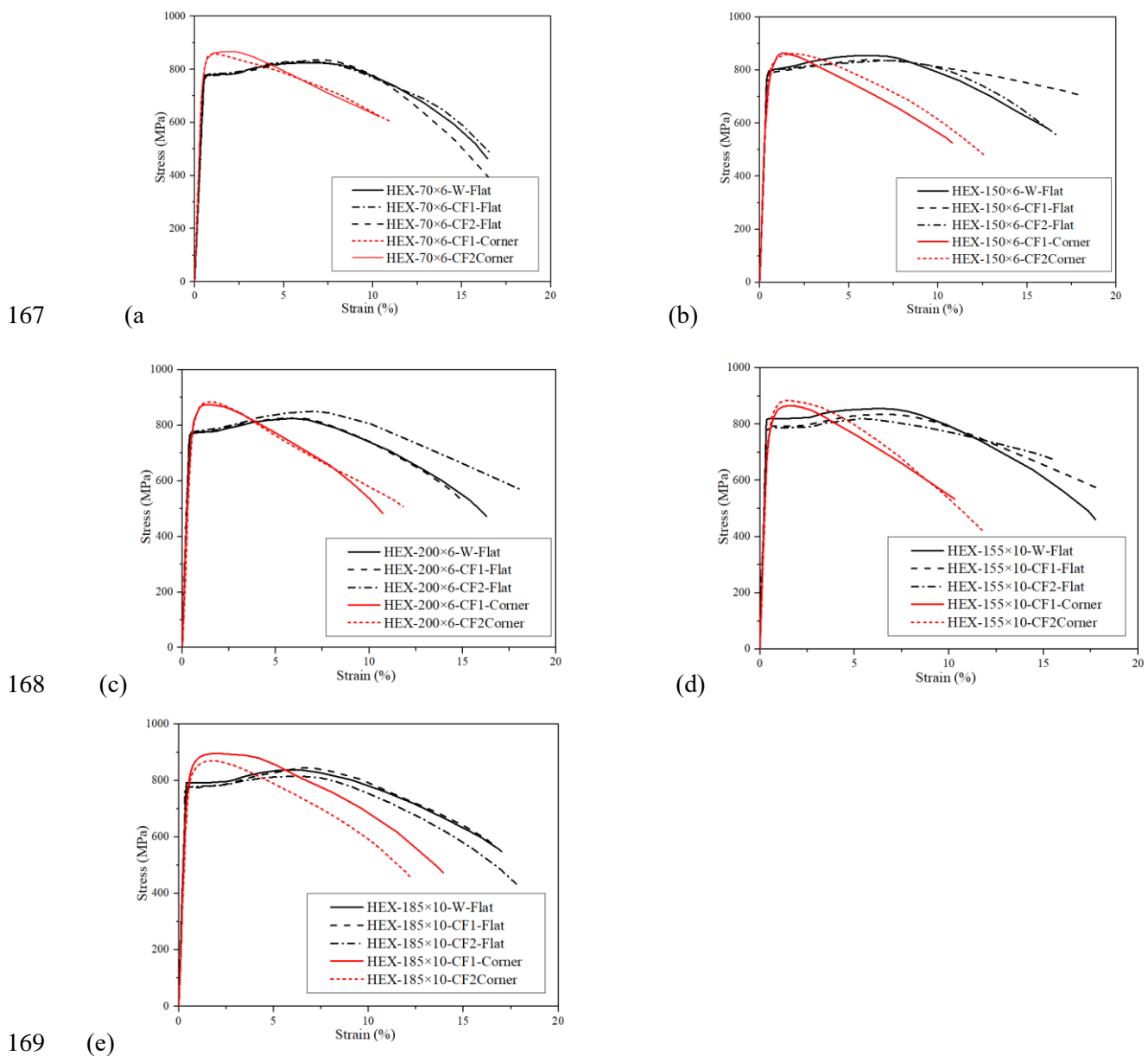


Fig. 5. Stress-strain curves of the tensile coupons taken from the HSS parent plates (a) 6 mm thick plate (b) 10 mm thick plate [15].

Table 2 Test results of the material properties of the flat coupons taken from the sections.

Section	$E_{s,f}$ (GPa)	$f_{y,f}$ (MPa)	$f_{u,f}$ (MPa)	$\varepsilon_{u,f}$ (%)	$\varepsilon_{f,ex,f}$ (%)	$\varepsilon_{f,f}$ (%)	$f_{0.05,f}$ (MPa)
HEX-70×6-W	218.9	778	825	7.2	16.3	16.5	776
HEX-70×6-CF1	209.8	780	828	5.9	16.6	17.1	767
HEX-70×6-CF2	214.5	776	826	6.6	16.8	15.9	773
HEX-150×6-W	209.4	782	822	6.8	16.5	16.2	776
HEX-150×6-CF1	206.5	775	810	6.0	17.7	16.8	772
HEX-150×6-CF2	211.2	780	822	6.8	16.2	16.5	761
HEX-200×6-W	206.5	771	824	6.1	16.4	17.2	767
HEX-200×6-CF1	213.2	773	826	6.0	14.9	15.5	774
HEX-200×6-CF2	211.6	780	832	6.9	19.4	17.8	772
HEX-155×10-W	214.5	792	835	6.9	17.6	17.1	790
HEX-155×10-CF1	216.3	779	837	6.2	17.8	17.5	775
HEX-155×10-CF2	206.2	788	830	5.1	15.5	16.6	785
HEX-185×10-W	214.3	787	828	6.4	16.6	17.3	785
HEX-185×10-CF1	204.8	781	827	6.5	16.8	16.5	778
HEX-185×10-CF2	205.7	777	815	6.2	17.8	17.2	773

160 Likewise, the measured material properties at flat and corner portion are tabulated in Tables 2 and 3
 161 respectively. Different letters were used to differentiate the locations where the tensile coupons were taken
 162 from the HSS HexHS. The letter “p” was used to indicate the material properties were derived from parent
 163 plates whereas the letters of “f” and “c” in subscript in Tables 2-3 indicate that the material properties were
 164 obtained from flat coupons and corner coupons. The determined stress-strain curves from flat- and corner
 165 portions corresponding to different series are depicted in Fig. 6 by which the effect of cold-forming
 166 manufacture process is highly elucidated by the stress-strain curves.



169 (e)
 170 Fig. 6. Measured material stress-strain curves of tensile coupons extracted from HSS HexHS stub columns.
 171

172 The stress-strain curves from flat coupons exhibit relatively limited yield plateau without sharply defined yield
173 point. For the corner coupons, the yield strength and ultimate strength were extensively increased due to the
174 press-braking process by which the corner portions undergone excessive degree of plastic strains. However,
175 the ductility of the corner coupons and elongation of fracture were both deteriorated.

176 2.3 Geometric imperfection

177 Initial local geometric imperfections are known to have negative impacts on the resistance and may trigger the
178 development of local buckling failure. Initial local geometric imperfections can be generated during the process
179 of manufacturing, transportation, and installation.

180

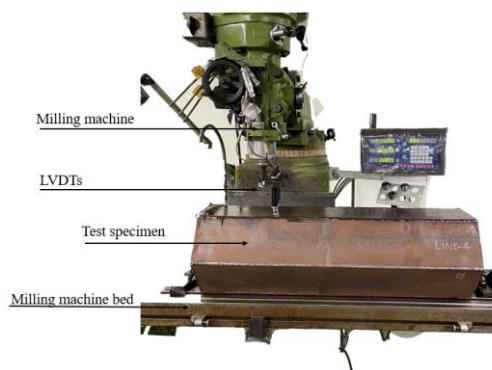
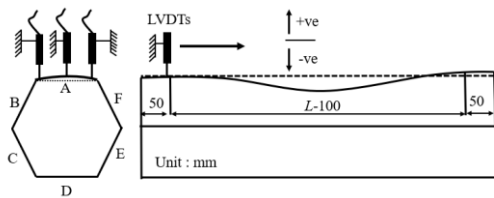
181 Table 3 Test results of the material properties of the corner coupons taken from the sections.

182	Section	$E_{s,c}$ (GPa)	$f_{y,c}$ (MPa)	$f_{u,c}$ (MPa)	$\varepsilon_{u,c}$ (%)	$\varepsilon_{f,ex,c}$ (%)	$\varepsilon_{f,c}$ (%)	$f_{0.05,c}$ (MPa)
183	HEX-70×6-CF1	198.2	812	865	1.5	10.4	10.8	752
	HEX-70×6-CF2	197.5	816	874	1.7	10.9	11.5	758
184	HEX-150×6-CF1	190.1	818	867	1.4	11.5	10.8	762
	HEX-150×6-CF2	190.4	813	876	1.3	10.6	11.4	736
185	HEX-200×6-CF1	195.5	815	872	1.6	11.2	10.9	756
	HEX-200×6-CF2	192.4	810	884	2.0	13.6	11.2	751
186	HEX-155×10-CF1	197.6	817	869	1.8	10.8	11.5	762
	HEX-155×10-CF2	200.2	821	882	1.7	11.7	12.6	749
187	HEX-185×10-CF1	210.3	816	893	2.5	13.9	12.5	735
	HEX-185×10-CF2	200.2	810	867	1.8	12.3	12.1	736

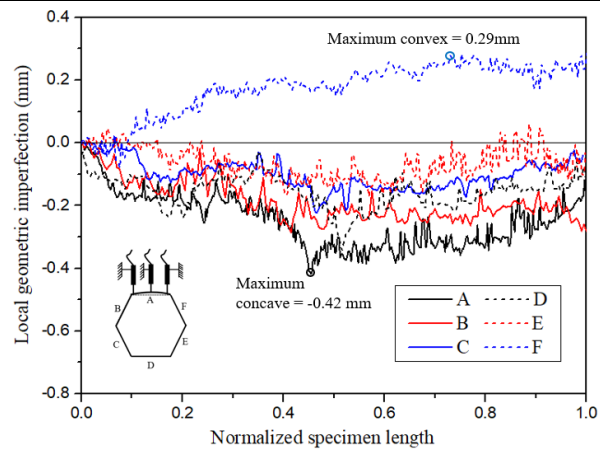
188

189 The magnitudes of the initial local geometric imperfection in HSS HexHS were thereby measured for each
190 stub column prior to the axial compression tests. For the measurements, all the HSS HexHS stub columns were
191 mounted to a milling machine as a measurement platform and a set of three Linear Variable Displacement
192 Transducers (LVDTs) were clamped and affixed to the head of milling machine. The test set-up and the
193 arrangement of the LVDTs are presented in Fig. 7 and similar set-ups were also adopted by Schafer and Peköz
194 [26] and Liu et al. [27]. The LVDTs with an accuracy of 0.001 mm were moving along the length of the

195 longitudinal direction of the specimen, with two LVDTs locating near the edge of the corner regions and one
 196 LVDT measured along the mid portion of the flat portion. It was worth mentioning that the 2 mm interval
 197 measurements were carried out and the measurements were commenced and stopped at a distance of 50 mm
 198 away from the specimen end to avert the possible local imperfections caused during the cutting process. The
 199 sign conventions of the measured local imperfections were also denoted in Fig. 7. For each plate element, the
 200 magnitude of the initial local geometric imperfection was defined as the deviation between the measurement
 201 at the mid-portion and a straight datum line connecting the measurements at the corners while the largest
 202 measured deviation among all six plate elements was defined as the initial geometric imperfections of the stub
 203 column specimen ω_o .
 204 A typical measured initial local geometric imperfection distribution profile along the six surfaces for the
 205 specimen HEX-70-6-W is depicted in Fig. 8. The measured amplitudes of the initial local geometric
 206 imperfection for all the HSS HexHS specimens are reported in Table 4 together with the measured dimensions.
 207 It is worth noting that the measured initial local geometric imperfection magnitudes from W-series are
 208 generally higher than those obtained from CF1- and CF2-series and the imperfection values exhibit an
 209 increasing tendency proportional to the cross-section dimensions of the investigated specimen.



210 (a)
 211 (b)
 212 Fig. 7. Set-up of local geometric imperfection measurement for HSS HexHS (a) Schematic configuration of
 213 the geometric imperfection measurement (b) Experimental arrangement of the geometric imperfection
 214 measurement.
 215



216
 217 Fig. 8. The distributions of local geometric imperfections along the length of HSS HexHS stub column
 218 specimen of HEX-70×6-W.

19

20

Table 4 Dimensions of the HSS HexHS stub columns

Section	Edge width B (mm)	Depth H (mm)	Side width b (mm)	Thickness t (mm)	Length L (mm)	Inner radius r_i (mm)	Welding w_r (mm)	Welding w_i (mm)	b/t (-)	Area A (mm ²)	ω_0 (mm)
HEX-70×6-W	71.6	137.9	51.6	5.91	390	- ^a	19.1	13.0	8.7	2456.7	0.42
HEX-70×6-CF1	71.7	136.5	46.7	5.90	390	18.0	19.6	12.5	7.9	2391.2	0.38
HEX-70×6-CF2	71.9	135.1	44.7	5.90	390	18.0	- ^b	- ^b	7.6	2345.7	0.35
HEX-70×6-CF2#	72.0	135.2	44.8	5.89	390	18.0	- ^b	- ^b	7.6	2342.5	0.39
HEX-150×6-W	152.9	301.9	135.3	5.89	870	- ^a	13.4	9.3	22.9	5404.6	0.50
HEX-150×6-CF1	150.2	294.5	125.4	5.90	870	18.0	19.5	12.5	21.3	5231.6	0.48
HEX-150×6-CF2	150.3	296.1	124.5	5.91	870	18.0	- ^b	- ^b	21.1	5249.5	0.45
HEX-150×6-CF2#	150.2	296.0	124.4	5.91	870	18.0	- ^b	- ^b	21.0	5250.2	0.46
HEX-200×6-W	206.3	406.7	187.9	5.89	1300	- ^a	17.1	9.7	31.9	7280.2	0.62
HEX-200×6-CF1	203.9	403.8	179.9	5.89	1300	18.0	17.6	11.2	30.5	7179.3	0.56
HEX-200×6-CF2	206.9	403.5	179.3	5.90	1300	18.0	- ^b	- ^b	30.4	7209.3	0.54
HEX-155×10-W	157.5	308.3	133.7	9.81	980	- ^a	18.3	10.2	13.6	9057.6	0.51
HEX-155×10-CF1	155.8	303.6	118.0	9.79	980	30.0	23.2	14.4	12.1	8824.3	0.46
HEX-155×10-CF2	156.3	296.7	110.1	9.80	980	30.0	- ^b	- ^b	11.2	8733.1	0.45
HEX-155×10-CF2#	156.8	296.9	110.3	9.81	980	30.0	- ^b	- ^b	11.2	8742.3	0.45
HEX-185×10-W	188.4	369.4	165.6	9.78	1150	- ^a	19.0	9.1	16.9	10866.9	0.57
HEX-185×10-CF1	184.9	356.2	151.1	9.80	1150	30.0	20.0	8.2	15.4	10532.2	0.51
HEX-185×10-CF2	186.8	356.4	139.5	9.81	1150	30.0	- ^b	- ^b	14.2	10516.1	0.54

21

22

Note: ^a indicates that cold-bent corners radius is not applicable for W-series HSS HexHS, ^b indicates the welding geometries at corner region are not applicable for CF2-series sections, and # indicates a repeated test specimen.

23

224 3. Stub column tests

225 3.1 Test setup and procedures

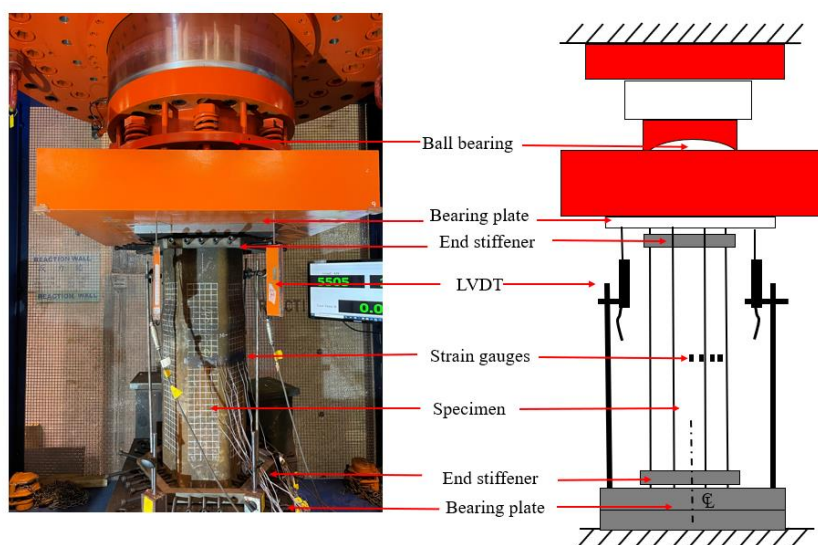
226 Tests on a total of 18 HSS HexHS stub column specimens under concentric compression loading were
227 conducted at the Structural Engineering Research Laboratory of The Hong Kong Polytechnic University, as
228 shown in Fig. 9. Prior to the testing, both ends for all the specimens were milled flat to ensure the uniform
229 distribution of the compressive load over the cross section. The length of the stub column was carefully
230 designed to be short enough to avoid global buckling but sufficiently long to encompass the representative
231 initial local geometric imperfections (at least three half-sinusoidal buckling waves) and residual stresses
232 pattern. To prevent the possible premature buckling failure near the ends of the specimen due to the highly
233 concentrated stress, a pair of specially developed end stiffeners with height of 30 mm were mounted to the
234 specimens clamping the section ends by a few of HSS bolts, as shown in Fig. 10. The tests were carried out
235 using a universal servo-controlled testing machine with the capacity of 25,000 kN. Four 50 mm range Linear
236 Variable Displacement Transducers (LVDTs) were located at four corners to measure the end shortening of the
237 stub columns, as presented in Fig. 10. Moreover, a total of 12 strain gauges were affixed to the mid height of
238 all specimens to capture the longitudinal strains and to detect the initiation of local buckling, if any. It was
239 worth mentioning that some of the strain gauges were located at which local buckling may most likely occur
240 (such as the mid portion of the plate elements corresponding to the peak of the amplitude of the half-sine
241 buckling wave). Furthermore, the strain gauges were also adhered to the locations at which distinct structural
242 characteristics induced by manufacturing process can be explicitly reflected. A displacement control with a
243 constant loading speed of $0.05\%L$ mm/min was used for the tests [12]. The loading rate provides a similar
244 strain rate to those used for the tensile coupon tests before yielding. Moreover, the readings from the strain
245 gauges were utilised to modify the initial stage of the LVDT readings, aiming to remove the effect of the initial
246 gaps and the elastic deformations from the end plates, by which true specimen end shortening can be derived

[27]. To ensure the correct testing instrumentation and the strain gauges can work well, an initial load (pre-load) at about 10% of the anticipated yield load was applied to the stub column prior to the formal testing. The key test results including the ultimate axial load N_u , the end shortening at ultimate load δ_u , yield load N_y , the ultimate to yield load ratio N_u/N_y and the ratio of local buckling load to yield load N_{lb}/N_y are reported in Table 5. It should be noticed that the yield load $N_y = A \times f_{y,m}$, where $f_{y,m}$ is the average yield strength weighted by the area of flat regions and corner regions for cold-formed section for CF1- and CF2-series, whereas the yield load $N_y = A \times f_y$ for HexHS with the fabrication route of “W” series, was taken as the average yield strength f_y measured for flat coupons. It should be noted that the weighted yield strength $f_{y,m}$ was used to determine whether the specimen is failed by cross-sectional yielding or local buckling. The ultimate to yield load ratio N_u/N_y was used to distinguish whether the specimen are failed by cross-section yielding or failed prior to the attainment of yield load due to local buckling. For the sections which failed by local buckling prior to the attainment of the yield load were named as slender sections and sections failed by yielding were categorised as non-slender sections. For the investigated HSS HexHS with same nominal cross-sectional dimensions, W-series specimens generally exhibit relatively lower normalised cross-sectional resistance than the CF-1 and CF-2 series. It may be primarily due to the fact that the cold-formed sections of CF-1 and CF-2 series featured shorter flat element width than W-series, particular for sections comprise 10 mm thick plate, the inner corner radius is 30 mm to avoid the fracture due to press-braking, which is significantly larger than the plate thickness. The cross-section resistance of cold-formed section series, particularly for CF-2 series benefit from the interaction effect from the constituent plate element with shorter length and enhanced strength induced by press-braking. In addition, extensive welding work were involved in fabrication process of W-series specimens, leading to comparably larger membrane residual stresses and heat affected zones, which may also reduce the ultimate resistance of the W-series specimens.

A photo of the deformed shapes of the failed stub column specimens with representative failure modes is shown

270 in Fig. 11. For those slender sections, typical inward-outward plate buckling is observed whereas the specimens
 271 feature yielding failure, the “elephant foot” buckling are observed. More specifically, specimens fabricated
 272 using different fabrication methods exhibit similar failure modes with same nominal cross-section dimensions
 273 and comparable cross-section resistance. The experimental test results of axial load-end shortening
 274 relationships recorded for the three series HSS HexHS specimens are plotted in Fig. 12. It is observed that
 275 prominent deformation capacities with desired ductility are remarkably associated with the load-end shortening
 276 curves for those sections failed by cross-section yielding. A relatively longer plateau maintaining the certain
 277 load-level after entering the path of plasticity are shown in the curves from the stocky sections, such as HEX-
 278 70×6-W, HEX-70×6-CF1, HEX-70×6-CF2, HEX-155×10-W, HEX-155×10-CF1 and HEX-155×10-CF2.
 279 Different from the observations for the specimens with stocky sections, the load-end shortening curves
 280 recorded from the sections failed by local buckling with the ultimate loads lower than the yield load show
 281 lower ductility and deformation capacity. For specimens such as HEX-150×6-W, HEX-150×6-CF1, HEX-
 282 150×6-CF2, HEX-200×6-W, HEX-200×6-CF1 and HEX-200×6-CF2, the material properties are not fully
 283 utilised in the sections due to the occurrence of local buckling and relatively quick drop in load are observed
 284 after reaching the ultimate cross-section resistance.

285



286

Fig. 9. Experimental arrangement of the HSS HexHS stub column tests with a specimen in place.

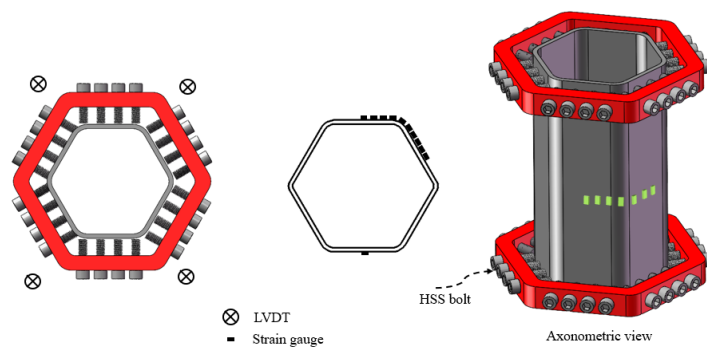


Fig. 10. Details of the strain gauges arrangement and the set-up of the end stiffeners.



Fig. 11. Photo of the selected failed HSS HexHS stub columns with representative failure modes.

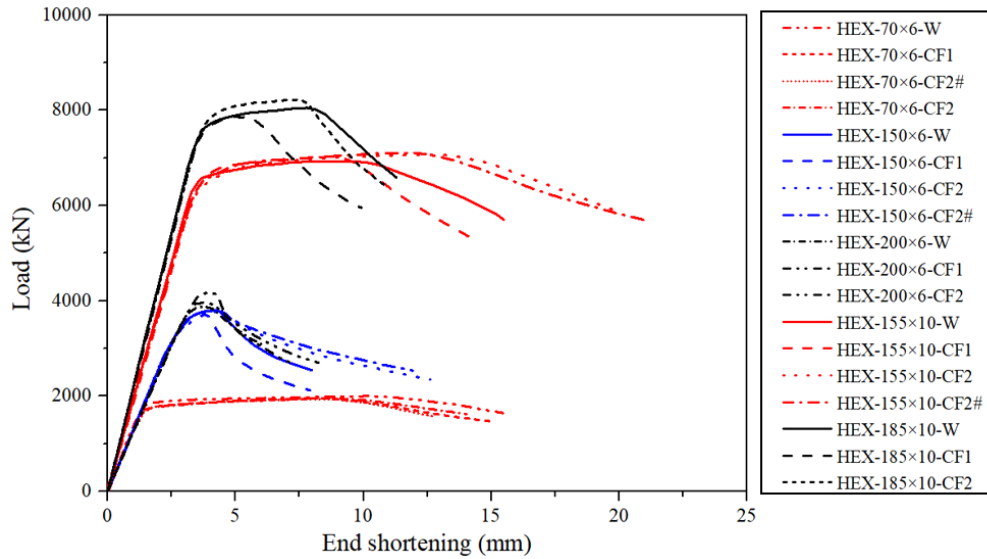
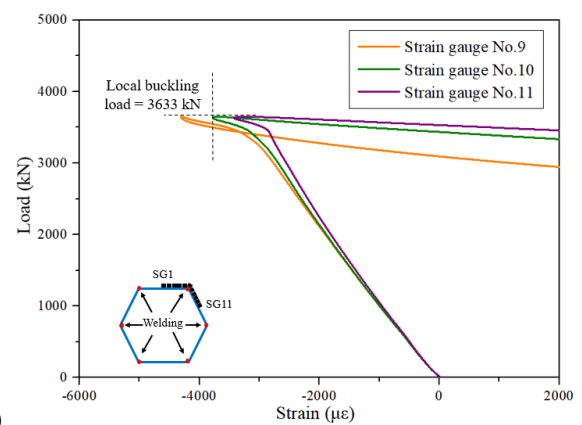
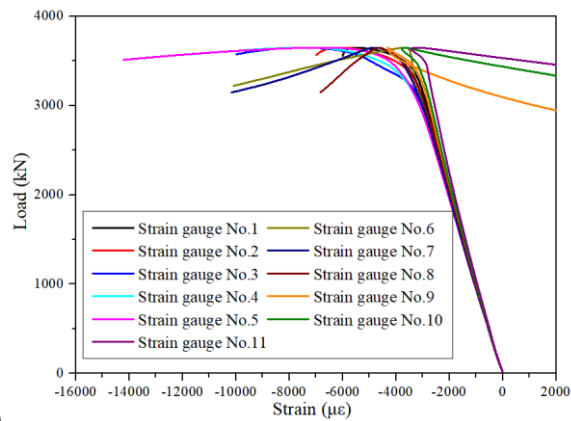


Fig. 12. Experimental and numerical load-end shortening curves of HSS HexHS stub columns.

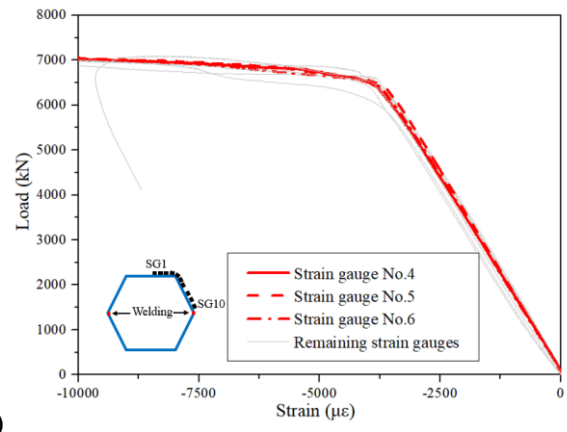
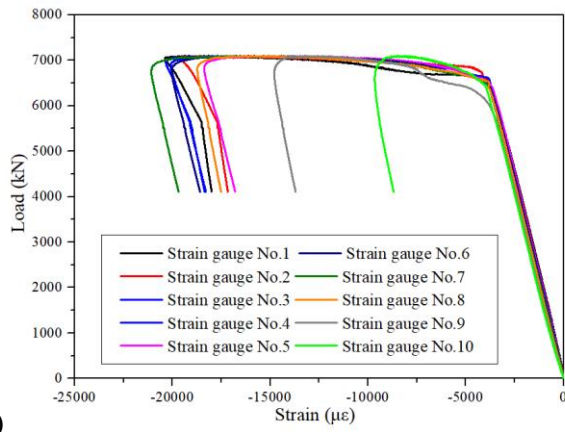
Aside from the load-end shortening diagrams, the relationship between the load and the longitudinal strain were also determined. Using the strain gauge readings, the local buckling load can be determined based on the strain reversal method [29], as shown in Fig. 13 marked with the dashed cross. The buckling load was determined for all the sections failed by local buckling (slender sections) and reported in Table 5 in a normalised form to the yield load N_{lb}/N_y . Compared with sections with relatively smaller dimensions, slender sections with larger dimensions generally show lower normalised buckling load ratio as anticipated. Fig. 14 demonstrates the load-strain relationship for the stub column specimen of HEX-155x10-CF1 which was failed by cross-section yielding.

As shown in Fig. 14, no strain gauge displays opposite increasing tendency until reaching the ultimate load, indicating that no local buckling failure has occurred during the entire loading process. Moreover, the load-strain curves corresponding to the strain gauges of NO.4, No.5 and No. 6 (highlighted in red) in the vicinity of the cold-bent corner region, show comparably higher stress levels in comparison to the load achieved from the other strain gauges under the same load level. This phenomenon is principally due to the press-braking process that hardened materials are located at corner regions with improved yield strengths.



(a) Complete load-strain curves (b) Determination of local buckling load

Fig. 13. Comparison of load-strain relationship of HSS HexHS stub column specimen HEX-150×6-W (a)



(a) (b)
Fig. 14. Comparison of load-strain relationship of HSS HextHS stub column specimen HEX-155×10-CF1 (a) Complete load-strain curves (b) Initial part of load-strain curves.

Table 5 Summary of the HSS HexHS stub column test results

Specimens	$N_{u,test}$ (kN)	δ_u (mm)	$N_{u,test}$ $/Af_{y,m}$	N_{lb} (kN)	N_{lb} $/Af_{y,m}$	Failure mode
HEX-70×6-W	1982	10.2	1.05	- ^a	N.A.	Yielding
HEX-70×6-CF1	1951	8.5	1.04	- ^a	N.A.	Yielding
HEX-70×6-CF2	1943	8.2	1.06	- ^a	N.A.	Yielding
HEX-70×6-CF2#	1944	8.3	1.06	- ^a	N.A.	Yielding
HEX-150×6-W	3648	4.3	0.88	3607	0.87	Local bucking
HEX-150×6-CF1	3754	3.8	0.92	3632	0.89	Local bucking
HEX-150×6-CF2	3806	4.4	0.93	3765	0.92	Local bucking
HEX-150×6-CF2#	3808	4.3	0.94	3686	0.91	Local bucking
HEX-200×6-W	3877	3.7	0.69	3765	0.67	Local bucking
HEX-200×6-CF1	3895	3.7	0.70	3672	0.66	Local bucking
HEX-200×6-CF2	4354	4.0	0.77	3964	0.71	Local bucking
HEX-155×10-W	7027	10.1	1.02	- ^a	N.A.	Yielding
HEX-155×10-CF1	7101	11.9	1.03	- ^a	N.A.	Yielding
HEX-155×10-CF2	7109	12.2	1.04	- ^a	N.A.	Yielding
HEX-155×10-CF2#	7186	11.2	1.04	- ^a	N.A.	Yielding
HEX-185×10-W	8143	7.8	0.98	7893	0.95	Local bucking
HEX-185×10-CF1	8052	5.3	0.99	7727	0.96	Local bucking
HEX-185×10-CF2	8402	7.1	1.03	- ^a	N.A.	Yielding

Note: ^a indicates local buckling load is not applicable to specimens failed by yielding; # indicates a repeated test specimen.

379 4. Evaluation of the current design methods

380 In this section, the applicability of the existing design provisions for internal plate members of SHS/RHS under
381 axial compression in commonly used structural steel design codes such as EN 1993-1-12 [21], ANSI/AISC
382 360-16 [22], AS 4100 [23] and EN 1993-1-5 [34] and the design rules of hexagonal hollow sections in
383 transmission pole design code are evaluated and assessed against the tested HSS HexHS stub columns. The
384 slenderness yield limits, and the cross-sectional resistance predictions were compared against the tested results.
385 In addition to the design codes assessment, design approaches of DSM and CSM which can take strain
386 hardening and element interaction effect into account were also evaluated.

387 4.1 Cross-section classification

388 The concept of cross-section classification and the methodology of the effective width method for cross section
389 experiencing local buckling for design of high strength steel hollow sections including conventional profile of
390 SHS, RHS, CHS is specified in European code of EN 1993-1-12 [21], ANSI/AISC 360-16 [22] and AS 4100
391 [23]. For hexagonal hollow sections, design code of ASCE/SEI 48-11 provides slenderness limits and design
392 provisions. It should be noted that EN 1993-1-12 allows for high strength steel design with nominal yield
393 strength greater than 460 MPa and up to 700 MPa and stems mostly from the design provisions of EN 1993-
394 1-1 [35] for normal strength mild steel. EN 1993-1-12 [21] adopts the same classification framework given in
395 EN 1993-1-1 [35]. For the cross-sections which can attain the yield of Af_y are classified as Class 1-3 sections,
396 whereas those sections failed to achieve the yield load due to the occurrence of local buckling are categorised
397 as Class 4. Similarly, the cross-section classification is also specified in codes of ANSI/AISC 360-16 [25] and
398 AS 4100 [26] and considers non-slender or slender sections for the sections that have the ultimate strength
399 above or below the yield load respectively. Thus, the slender sections can be considered as the corresponding
400 Class 4 sections and non-slender sections are those Class 1-3 sections. The cross-section slenderness based on
401 the width-to-thickness ratio or diameter-to-thickness ratio is used as a governing parameter for cross section

classification under compression. To determine the cross-section slenderness, different material parameters are used in different design codes, such as $\varepsilon_{EC3} = (235/f_y)^{0.5}$, $\varepsilon_{AISC} = (E/f_y)^{0.5}$, and $\varepsilon_{AS4100} = (250/f_y)^{0.5}$ used to account for the differences of the material strengths in various codes respectively. Based on previous experimental studies carried out for octagonal hollow sections (OctHS) of conventional strength steel with nominal yield strength $f_y = 355$ MPa [14] and high strength steel with nominal yield strength $f_y = 460$ MPa [12] and $f_y = 690$ MPa [2], plate buckling theory for internal compression elements have been assessed and demonstrated to be applicable to be extended for octagonal sections, which thus may be suitable for the hexagonal sections studied in this paper. Cross-section slenderness limits stipulated in structural steel design codes of EN 1993-1-12, AS 4100, ANSI/AISC 360-16 and EN 1993-1-5 [34] for internal plate element and design code of ASCE/SEI 48-11 under compression are summarised in Table 6. For simple and direct comparison, the normalised form of plate slenderness $\lambda_{lim} = (b/t)(f_y/E)^{0.5}$ specified in ANSI/AISC 360-16 was used as a standard expression to harmonise the different expressing forms in EN 1993-1-12, AS 4100 and ASCE/SEI 48-11. In line with the design codes, the direct strength method (DSM), which is applicable to arbitrary cross sections for critical elastic buckling stress prediction was also assessed for its applicability for design strength predictions for HSS HexHS. For HexHS stub column, neither global buckling nor distortional buckling was observed. The nominal axial strength predicted by DSM was thereby taking by the nominal strength of HexHS for local buckling. The DSM utilises an overall cross-section slenderness λ_p defined in Eq. (1) to determine the cross-sectional capacity, where f_y is the yield strength of the steel material and f_{cr} is the critical elastic buckling stress. To determine the nominal axial strength for local buckling, the critical elastic local buckling load can be obtained from CUFSM [30] program using the finite strip method or finite element program ABAQUS [31] and was subsequently substituted into the DSM design equation. In DSM, the sections with cross-section slenderness λ_p greater than 0.776 cannot reach the yield load, this value was thus considered to be the cross-section classification limit based on DSM.

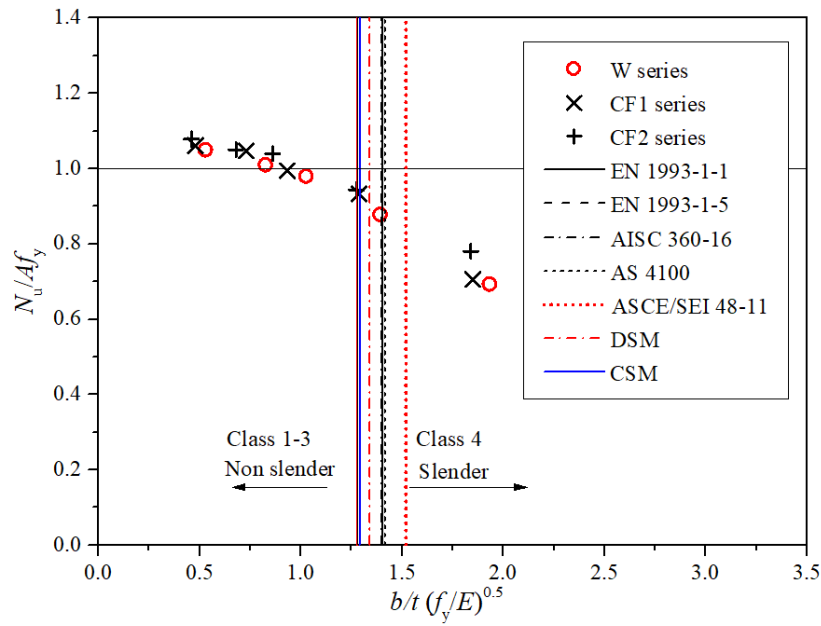


Fig. 15. Assessment of the slenderness yield limits in the design codes and design approaches

In addition to the DSM design approach, a deformation-based design method - continuous strength method (CSM), accounting for the strain hardening of the metallic material and the effect of the element interaction [32–33] was also considered and evaluated in this study.

$$\lambda_p = \sqrt{f_y / f_{cr}}$$

(1)

The iteration of the effective area of the cross section and cross-section classification is not needed in the design of strength predictions. The stipulated cross-section yield slenderness from design codes of EN 1993-1-1, AS 4100, ANSI/AISC 360-16, EN 1993-1-5 and ASCE/SEI 48-11 were converted to 1.405, 1.414, 1.400, 1.279 and 1.520 respectively. It is worth mentioning that AISI S100-16 [31] specifies close yield slenderness limit value of 1.280 as EN 1993-1-5, though different cross-section slenderness definition and equation was adopted in AISI S100. Similarly, the yield slenderness limits from DSM and CSM design approaches were also converted with values of 1.470 and 1.290 respectively. The assessment was carried out by normalising the

441 N_u from experimental investigations with the corresponding yield load Af_y , where f_y was taken as the average
442 yield strength from the flat coupons, in compliance with the commonly adopted design process. The normalised
443 N_u was then plotted against the normalised plate slenderness λ_{lim} of the governing plate element, as shown in
444 Fig. 15.

445

446

447

448

449

450 Table 6 Summary of the cross-section yield slenderness limits in design codes and design approaches

Design standards and methods	Yield slenderness limits	λ_{lim}
EN 1993-1-12 [22]	$b/t \leq 42\epsilon_{EC3}$, $\epsilon_{EC3} = \sqrt{235 / f_y}$, $E = 210$ GPa	1.405
ANSI/AISC 360-16 [23]	$b/t \leq 1.40\epsilon_{AISC}$, $\epsilon_{AISC} = \sqrt{E / f_y}$, $E = 200$ GPa	1.400
EN 1993-1-5 [34]	$\bar{\lambda}_p = \frac{b/t}{28.4\epsilon\sqrt{k}} \leq 0.5 + \sqrt{0.085 - 0.055\psi} = 0.673$, $\psi = 1$ for pure compression, $\epsilon_{EC3} = \sqrt{235 / f_y}$, $k = 4$, $E = 210$ GPa	1.279
AS 4100 [24]	$b/t \leq 14\epsilon_{AS4100}$, $\epsilon_{AS4100} = \sqrt{250 / f_y}$, $E = 200$ GPa	1.414
ASCE/SEI 48-11 [21]	$b/t \leq 681.2 / \sqrt{f_y}$, $E = 200$ GPa	1.520
DSM	$\lambda_p = \sqrt{f_y / f_{cr}} \leq 0.776$, $E = 200$ GPa	1.470
CSM	$\lambda_p = \sqrt{f_y / f_{cr}} \leq 0.68$, $E = 200$ GPa	1.290

451

452

453

454 Based on the comparisons between the test data and the converted cross-section yield limits, it is obvious that
455 the yield slenderness limits in the existing structural steel design codes are located on the unsafe side. The data
456 points converge to the unity with a slenderness value far away from the intersections between the unity and
457 the design codes as well as the design approaches. This indicates that the yield slenderness limit specified for

internal plate members in EN 1993-1-12, AS 4100 and ANSI/AISC 360-16 and hexagonal sections in ASCE/SEI 48-11 cannot be extended to cover the design of HSS HexHS. Furthermore, the HSS HexHS with different fabrication routes exhibit comparably different normalised values with similar plate slenderness, indicating that respective classification limits need to be further proposed.

4.2 Cross-section capacity

For the structural elements failed prior to the attainment of yielding strength by local buckling failure, the effective width method is utilised in current design codes in EN 1993-1-5 [34], ANSI/AISC 360-16 [22] and AS 4100 [23]. For cross-section resistance predictions the ultimate strength predictions from the design codes were determined using the average yield strength f_y from the flat coupons. For the sections undergone local buckling, the dimension of the side width b of the slenderest plate within the section of the cross-section is reduced to the effective width b_{eff} whereupon resulting in an effective compressive resistance $A_{\text{eff}}f_y$, where A_{eff} is the effective area of the section. Though effective width concept is used in these three design codes, different equations were adopted to determine the effective width of the sections. The formulae of the effective width equations adopted in EN 1993-1-5 [34] are given in Eq. (2).

$$\frac{b_{\text{eff,EC3}}}{b} = \begin{cases} 1 & \text{for } \bar{\lambda}_p \leq 0.673 \\ \left(1 - 0.22 / \bar{\lambda}_p\right) / \bar{\lambda}_p & \text{for } \bar{\lambda}_p > 0.673 \end{cases} \quad (2)$$

where $\bar{\lambda}_p$ is the plate slenderness which can be obtained in accordance with EN 1993-1-5 [34] as shown in Eq. (3), and buckling factor k_σ is equal to 4.0 for the plate element under compression.

$$\bar{\lambda}_p = \frac{b/t}{28.4 \varepsilon_{\text{EC3}} \sqrt{k_\sigma}} \quad (3)$$

Unlike the multi-stage effective width method used in EN 1993-1-5, a single expression is used in AS 4100 with a material coefficient $(250/f_y)^{0.5}$ used to account for the material difference and the width to thickness ratio b/t , as shown in Eq. (4)

$$\frac{b_{\text{eff,AS4100}}}{b} = \frac{40}{b / (t \varepsilon_{\text{AS4100}})} \quad (4)$$

The effective width provision in AISC 360-16 is correlated to the parameters of the limiting width to thickness ratio $\lambda_{\text{p,AISC}}$ and the width to thickness ratio b/t , as given in Eq. (5). The limiting width to thickness ratio $\lambda_{\text{p,AISC}}$ stipulated in design code of ANSI/AISC 360-16 for internal plate element is $1.4(E/f_y)^{0.5}$. It was worth mentioning that the clear width of the flat element excluding the corner regions are needed to derive the width to thickness ratio.

$$\frac{b_{\text{eff,AISC}}}{b} = \frac{1.38\lambda_{\text{p,AISC}}}{\lambda} - \frac{0.38\lambda_{\text{p,AISC}}^2}{\lambda^2} \quad (5)$$

In addition to the above discussed structural steel design codes, design code of transmission pole structures ASCE/SEI 48-11 which stipulates the design provisions concerning HexHS was also evaluated herein, as shown in Eq. (6)

$$f_{\text{a,ASCE}} = \begin{cases} f_y & \text{for } \frac{b}{t} \leq \frac{681.2}{\sqrt{f_y}} \\ 1.42f_y \left(1 - \frac{0.00114}{2.62} \frac{b\sqrt{f_y}}{t}\right) & \text{for } \frac{681.2}{\sqrt{f_y}} \leq \frac{b}{t} \leq \frac{919.6}{\sqrt{f_y}} \\ 4 \frac{\pi^2 E}{12(1-\nu^2)} \left(\frac{t}{b}\right)^2 & \text{for } \frac{919.6}{\sqrt{f_y}} \leq \frac{b}{t} \end{cases} \quad (6)$$

where A is the gross cross-section area, $f_{\text{a,ASCE}}$ is the effective compressive strength, f_y is the yield strength and b is the clear side width excluding corner portion.

As for the predicted compressive strength for the cross section governing by local buckling failure mode from DSM, the design equations related the capacity to the overall slenderness as given in Eq. (7).

$$N_{\text{DSM}} = \begin{cases} f_y A & \text{for } \lambda_p \leq 0.776 \\ \left(1 - \frac{0.15}{\lambda_p^{0.8}}\right) \frac{1}{\lambda_p^{0.8}} f_y A & \text{for } \lambda_p > 0.776 \end{cases} \quad (7)$$

In terms of the cross-section predictions for CSM, base-curve proposed for HSS RHS/SHS [37] in Eq. (9) are

497 used. The two upper limits are adopted to avoid over-prediction of ultimate capacity of non-slender cross
 498 sections, whilst the first limit corresponded to the structural ductility requirement in EN 1993-1-1 [35].

$$499 \quad \frac{\varepsilon_{\text{csm}}}{\varepsilon_y} = \begin{cases} \frac{0.294}{\lambda_p^{3.174}} \leq \min\left(15, \frac{C_1 \varepsilon_u}{\varepsilon_y}\right) & \text{for } \lambda_p \leq 0.68 \\ \left(1 - \frac{0.219}{\lambda_p^{1.014}}\right) \frac{1}{\lambda_p^{1.014}} & \text{for } 0.68 < \lambda_p \leq 2.61 \end{cases} \quad (8)$$

500 where $(\varepsilon_{\text{csm}}/\varepsilon_y)$ is the deformation capacity, ε_{csm} is the CSM limiting strain, ε_y is the yield strain which can be
 501 determined as f_y/E . To obtain the cross-section capacity, the linear strain hardening model proposed in [32] was
 502 used for HSS steel material with corresponding factors C_1 , C_2 equal to 0.40, 0.45 respectively. The quad-linear
 503 material model proposed in [33] was used for W-series sections. It is worth mentioning that the strain hardening
 504 of the corner portions was also incorporated in the cross-sectional resistance calculation of CSM with the
 505 assumption that the corner portions experienced the same ε_{csm} as the flat portions. The limiting stress f_{csm}
 506 applicable to CSM, is related to the CSM strain as given in Eq. (9).

$$507 \quad f_{\text{csm}} = \begin{cases} E_s \varepsilon_{\text{csm}} & \text{for } \varepsilon_{\text{csm}} \leq \varepsilon_y \\ f_y + E_{\text{sh}} (\varepsilon_{\text{csm}} - \varepsilon_{\text{sh}}) & \text{for } \varepsilon_y < \varepsilon_{\text{csm}} < C_1 \varepsilon_u \end{cases} \quad (9)$$

508 where E_s is Young's modulus, f_y is the yield stress, ε_y and ε_u are the strains at the yield and ultimate stresses,
 509 ε_{sh} is the strain hardening magnitude denoted as the end of the yield plateau. The strain hardening initiates after
 510 achieving this strain and $C_1 \varepsilon_u$ represents the strain at the intersection point between third stage of the material
 511 model and the measured stress-strain curve. The coefficient of C_1 is used to avert the over-predictions of
 512 material strength as a cut-off strain and the hardening modulus can be derived from Eq. (10). It should be noted
 513 that the measured f_y/f_u ratios result in extremely low ultimate strain than the test results according to the
 514 empirical equation in Buchanan et al. [32]. Thus, the expressions proposed by Yun et al. [33] were adopted for
 515 both material with and without yield plateau.

$$516 \quad E_{\text{sh}} = \frac{f_u - f_y}{C_2 \varepsilon_u - \varepsilon_y} \quad (10)$$

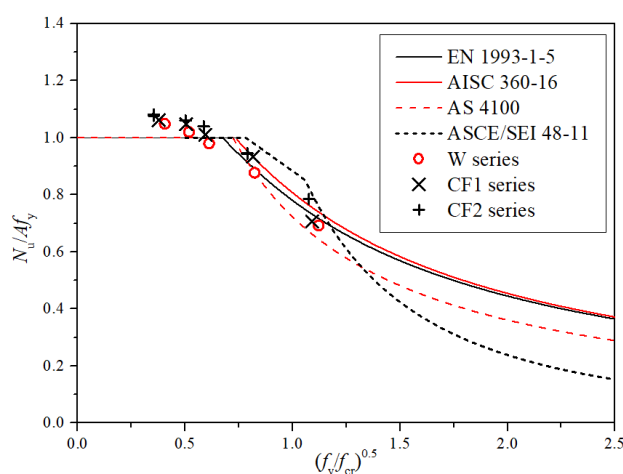
517 According to the CSM design approach, the stocky sections with cross-section slenderness lower than 0.68,
518 are largely benefited from the material strain hardening. For those specimens, the cross-section strength is
519 determined based on the CSM limiting stress and the gross area A , whereas the deformation capacity of $(\varepsilon_{\text{csm}}/\varepsilon_y)$
520 is used to determine the cross-section strength for specimens with slenderness greater than 0.68, as shown in
521 Eq. (11).

$$522 \quad N_{\text{csm}} = \begin{cases} f_{\text{csm}} A & \text{for } \lambda_p \leq 0.68 \\ \frac{\varepsilon_{\text{csm}}}{\varepsilon_y} f_y A & \text{for } \lambda_p > 0.68 \end{cases} \quad (11)$$

523 4.3 Assessment of the cross-section resistance

524 The cross-section resistances were assessed with the predicted values from the current design codes of EN
525 1993-1-12, AS 4100 and ANSI/AISC 360-16, ASCE/SEI 48-11 as well as the predictions from the design
526 approaches of DSM and CSM with all partial factors set to unity for direct comparison. The determined tested
527 strength-to-predicted ($N_{\text{u,test}}/N_{\text{u,pred}}$) ratios and the corresponding coefficient of variations (CoVs) are reported
528 in Table 7. The mean values of $N_{\text{u,test}}/N_{\text{u,pred}}$ from the method of EN 1993-1-12, AS 4100, ANSI/AISC 360-16,
529 ASCE/SEI 48-11, DSM and CSM are 0.98, 0.99, 0.99, 0.99, 0.99 and 1.00 with corresponding coefficient of
530 variations (CoVs) of 0.07, 0.06, 0.07, 0.07, 0.06 and 0.03 respectively.

531



532
533

Fig. 16. Assessment of the effective width methods in design codes.

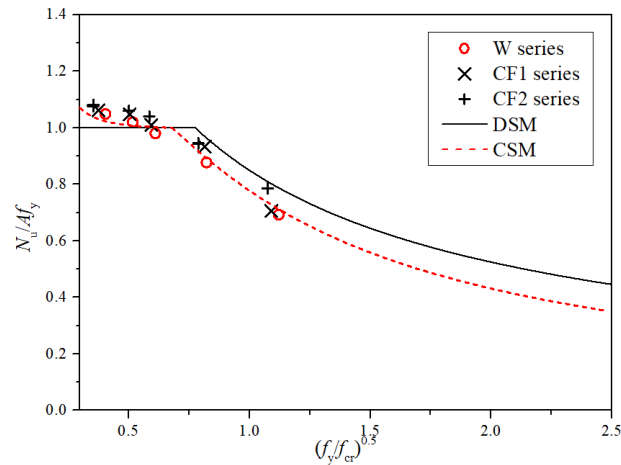


Fig. 17. Assessment of the design approaches DSM and CSM.

535

536

537

538

539

540

541

542

543

544

545

546

547

548

549

550

551

To further analyse the cross-section strengths of HSS HexHS failed by either cross-section yielding or local buckling, the values of the mean test-to-predicted and the corresponding CoVs are also assessed separately. In terms of the stocky cross sections failed by cross-section yielding, as anticipated, the design methods from EN 1993-1-12, AS 4100, ANSI/AISC 360-16, ASCE/SEI 48-11 and DSM underestimate the cross-section resistances, with mean $N_{u,test}/N_{u,pred}$ value of 1.05, 1.03, 1.05, 1.04 and 1.04 due to the neglect of strain hardening whereas the CSM gives better prediction with a mean value of 1.01 and corresponding CoV of 0.01. As for slender sections, the design codes generally tend to overestimate the cross-section strength. The mean value of $N_{u,test}/N_{u,pred}$ ratio based on EN 1993-1-12, AS 4100 and ANSI/AISC 360-16 provide comparably close mean values of $N_{u,test}/N_{u,pred}$ with 0.92, 0.93 and 0.93 respectively. Fig. 16 plot the relationship between the normalised test load and the cross-section slenderness with effective width equation from various design codes incorporated. It can be seen that design curves for slender sections subject to local buckling from EN 1993-1-5 and AISC 360-16 locate slightly higher than AS 4100 resulting in un-conservative predictions when the λ_p is greater than 0.82. The design curve from ASCE/SEI 48-11 is significantly higher than the counterparts from EN 1993-1-5, AS 4100, and ANSI/AISC 360-16, thereby leading to over-estimated predictions for the slender cross-sections. Though the design curves and design provisions from those design codes are different and

deviate from the test data at large, comparably close statistic results are still observed for section failed by local buckling, mainly due to the small number of test specimens and the inappropriate cross-section classification slenderness limit value. For cross-sectional strength predictions from design approaches, CSM provide more accurate predictions than the DSM, which can be demonstrated in Fig. 17, that design curve of CSM correlate well with most of the data point from slender sections of HexHS whereas DSM provide over-predicted cross-section strength. Overall, all three design codes generate over-conservative predictions due to the neglect of strain hardening. AS 4100 provides more accurate results compared with the EN 1991-1-12, AISC 360-16 and ASCE/SEI 48-11. Though CSM can provide more accurate predictions than the other design methods accounting for the strain hardening of the materials, the base curve may also need to be further developed for HSS HexHS.

Table 7 Comparison between the experimental test results with the predicted cross-section resistance for HSS HexHS from various design approaches.

Specimens	$N_{u,test}$ / $N_{u,EC3}$	$N_{u,test}$ / $N_{u,AISC}$	$N_{u,test}$ / $N_{u,AS4100}$	$N_{u,test}$ / $N_{u,ASCE}$	$N_{u,test}$ / $N_{u,DSM}$	$N_{u,test}$ / $N_{u,CSM}$
HEX-70×6-W	1.05	1.05	1.05	1.05	1.05	1.02
HEX-70×6-CF1	1.06	1.06	1.06	1.06	1.06	1.02
HEX-70×6-CF2	1.07	1.07	1.07	1.07	1.08	1.02
HEX-70×6-CF2#	1.08	1.08	1.08	1.08	1.08	1.02
HEX-150×6-W	0.91	0.99	0.88	0.91	0.91	0.98
HEX-150×6-CF1	0.93	0.98	0.93	0.93	0.96	1.04
HEX-150×6-CF2	0.94	0.99	0.94	0.94	0.95	1.03
HEX-150×6-CF2#	0.94	0.94	0.94	0.94	0.95	1.03
HEX-200×6-W	0.87	0.84	0.93	0.87	0.88	0.97
HEX-200×6-CF1	0.86	0.83	0.91	1.02	0.88	0.96
HEX-200×6-CF2	0.91	0.88	0.95	0.86	0.92	1.01
HEX-155×10-W	1.00	1.00	0.99	1.00	0.99	0.98
HEX-155×10-CF1	1.05	1.05	1.05	1.05	1.05	1.03
HEX-155×10-CF2	1.04	1.04	1.04	1.04	1.04	1.02
HEX-155×10-CF2#	1.04	1.04	1.04	1.04	1.04	1.02
HEX-185×10-W	0.95	0.95	0.95	0.95	0.96	0.95
HEX-185×10-CF1	0.95	0.95	0.96	0.95	0.96	0.95
HEX-185×10-CF2	1.02	1.02	1.01	1.01	1.01	1.00
Mean	0.98	0.99	0.99	0.99	0.99	1.00
CoV	0.07	0.07	0.06	0.07	0.06	0.03
Mean ^Y	1.05	1.05	1.03	1.04	1.04	1.01

CoV ^Y	0.02	0.02	0.04	0.02	0.03	0.01
Mean ^{LB}	0.92	0.93	0.93	0.91	0.93	1.00
CoV ^{LB}	0.03	0.06	0.03	0.05	0.03	0.03

Note: # indicates a repeated test specimen

565

5. Conclusions

A total of 18 HSS HexHS stub columns including three fabrication routes were performed under concentric compressive loads to examine the local buckling behaviour and the cross-section resistance. The material properties were measured by extracting the tensile coupons within the cross-sections. Initial local geometric imperfections were measured for each stub column specimen. Failure modes of the stub columns specimens were found to feature with typical plate buckling failure mode and yielding failure near the section ends. In terms of the cross-section resistance, relatively larger normalised cross-section resistance and deformation capacities were obtained for those stocky sections whereas slender sections failed by local buckling with normalised cross-section strength lower than the unity were accompanied by a sharp drop after achieving the ultimate load. The obtained test results were also compared with the existing design codes to assess the applicability of the design codes to the HSS HexHS. Moreover, the cross-section resistance determined in accordance with the design codes were evaluated for the investigated specimens. The experimental studies presented in this paper allow the following conclusions to be made:

(a) The initial local geometric imperfections are proportional to the cross-section slenderness and HSS HexHS fabricated by welding six plates may have relatively higher initial imperfection magnitudes than cold-formed sections.

(b) The yield slenderness limits for the cross-section classification in the existing structural steel design codes cannot be extended for application to HSS HexHS stub column under pure compression in this study.

(c) All design codes provide consistent but over-conservative cross-section resistance predictions for compact sections. Design code of AS 4100 provide more accurate predictions for the slender sections susceptible to

586 local buckling compared with design codes of EN 1993-1-12, AISC 360-16 and ASCE/SEI 48-11.

587 (d) In terms of the design approaches, CSM provide more accurate results compared with DSM due to the

588 consideration of strain hardening of metallic materials for stocky sections failed by cross-section yielding. The

589 cross-section resistances of the slender sections were over-estimated by DSM while CSM comparably provide

590 more accurate predictions than DSM.

591 (e) Though CSM yield relatively accurate results than DSM, a more suitable base curve and the material model

592 applicable to CSM may need further evaluation. A suitable slenderness yield limit should be proposed based

593 on the extensive parametric study which is currently under way.

594

595 **Acknowledgement**

596 The research work presented in this paper was supported by the Research Grants Council of the Hong Kong

597 Special Administrative Region, China (Project no. 15218918). The authors would also like to thank the

598 technical staff, Mr. C. F. Cheung, Mr. M. C. Ng and Mr. K. L. Cheung of the Structural Engineering Research

599 Laboratory.

600

601 **Data Availability Statement**

602 Some or all data that support the findings of this study are available from the corresponding author upon

603 reasonable request.

604

605 **References**

- 606 [1] Ma J-L, Chan T-M, Young B. Experimental Investigation on Stub-Column Behavior of Cold-Formed High-
- 607 Strength Steel Tubular Sections. J Struct Eng. 2016;142:04015174.
- 608 [2] Fang H, Chan T-M, Young B. Behavior of Octagonal High-Strength Steel Tubular Stub Columns. J Struct
- 609 Eng. 2019;145.

610 [3] Chen J, Chan T-M, Varma AH. Stub Column Behavior of Cold-Formed High-Strength Steel Circular
611 Hollow Sections under Compression. *J Struct Eng.* 2020;146:04020277.

612 [4] Chan TM, Gardner L. Compressive resistance of hot-rolled elliptical hollow sections. *Eng Struc.*
613 2008;30:522-32.

614 [5] Chan TM, Gardner L. Bending strength of hot-rolled elliptical hollow sections. *J Constr Steel Res.*
615 2008;64:971-86.

616 [6] Chan TM, Gardner L. Flexural Buckling of Elliptical Hollow Section Columns. *J Struct Eng.*
617 2009;135:546-57.

618 [7] Zhu J-H, Young B. Cold-Formed-Steel Oval Hollow Sections under Axial Compression. *J Struct Eng.*
619 2011;137:719-27.

620 [8] Chen M-T, Young B. Cross-sectional behavior of cold-formed steel semi-oval hollow sections. *Eng Struc.*
621 2018;177:318-30.

622 [9] Chen M-T, Young B. Tests of Cold-Formed Steel Semi-Oval Hollow Section Members under Eccentric
623 Axial Load. *J Struct Eng.* 2020;146.

624 [10] Liu JZ, Fang H, Chan TM. Experimental and numerical investigations on stub column behaviour of cold-
625 formed high strength steel irregular octagonal hollow sections. *Thin-Walled Struct.* 2022;

626 [11] Liu JZ, Fang H, Chan TM. Experimental investigation on material properties and residual stresses in cold-
627 formed high strength steel irregular octagonal hollow sections. *J Constr Steel Res.* 2022;191:107170.

628 [12] Chen J, Zhu J-Y, Chan T-M. Experimental and numerical investigation on stub column behaviour of cold-
629 formed octagonal hollow sections. *Eng Struc.* 2020;214:110669.

630 [13] Chen JB, Liu HX, Chan TM. Material properties and residual stresses of cold-formed octagonal hollow
631 sections. *J Constr Steel Res.* 2020;170.

632 [14] Zhu JY, Chan TM, Young B. Cross-sectional capacity of octagonal tubular steel stub columns under
633 uniaxial compression. *Eng Struc.* 2019;184:480-94.

634 [15] Liu J-z, Fang H, Chen S, Chan T-M. Material properties and residual stresses of high strength steel
635 hexagonal hollow sections. *J Constr Steel Res.* 2022;190:107061.

636 [16] Liu J-z, Fang H, Chan T-M. Investigation on material properties and residual stresses in cold-formed high
637 strength steel irregular hexagonal hollow sections. *Thin-Walled Struct.* 2022;176:109220.

638 [17] Aoki T, Migita Y, Fukumoto Y. Local buckling strength of closed polygon folded section columns. *J Constr*
639 *Steel Res.* 1991;20:259-70.

-
- 640 [18] Migita Y, Aoki T, Fukumoto Y. Local and interaction buckling of polygonal section steel columns. J Struct
641 Eng. 1992;118:2659-76.
- 642 [19] Godat A, Legeron F, Bazonga D. Stability investigation of local buckling behavior of tubular polygon
643 columns under concentric compression. Thin-Walled Struct. 2012;53:131-40.
- 644 [20] Liu J-z, Fang H, Chan T-M. Experimental investigations on material properties and stub column behaviour
645 of high strength steel irregular hexagonal hollow sections. J Constr Steel Res. 2022; 107343.
- 646 [21] ASCE/SEI 48-11, Design of steel transmission pole structures. Reston, Virginia: American Society of
647 Civil Engineers; 2011.
- 648 [22] EN 1993-1-12, Eurocode 3: Design of Steel Structures – Part 1–12: Additional Rules for the Extension of
649 EN 1993 up to Steel Grades S700. Brussels: European Committee for Standardization (CEN); 2007.
- 650 [23] ANSI/AISC 360-16, Specification for Structural Steel Buildings. Chicago: American Institute of Steel
651 Construction (AISC); 2016.
- 652 [24] AS 4100-1998(R2016), Steel structures (Reconfirmed 2016 Incorporating Amendment No.1), AS 4100.
653 Sydney, Australia: Australian Standard; 2016.
- 654 [25] EN ISO 6892-1, Metallic Materials – Tensile Testing Part 1: Method of Test at Ambient Temperature.
655 EN ISO 6892-1. Brussels, Belgium: CEN; 2019.
- 656 [26] Schafer B, Peköz T. Computational modeling of cold-formed steel: characterizing geometric
657 imperfections and residual stresses. J Constr Steel Res. 1998;47:193-210.
- 658 [27] Liu J-z, Chen S, Chan T-M. Testing, numerical modelling and design of Q690 high strength steel welded
659 T-section stub columns. Eng Struc. 2022;259:114142.
- 660 [28] Liu J-z, Chen S, Chan T-M. Experimental and numerical investigations of hybrid high strength steel
661 welded T-section stub columns with Q690 flange and Q460 web. Thin-Walled Struct. 2022; 177: 109403.
- 662 [29] Hu, P.C., Lundquist, E.E. and Batdorf, S.B. Effect of small deviations from flatness on effective width
663 and buckling of plates in compression, NACA TN 1124. National advisory committee for aeronautics; 1946.
- 664 [30] AISI S100-16, North American Specification for the Design of Cold-Formed Steel Structural Members.
665 Washington, DC, USA: AISI (American Iron and Steel Institute); 2016.
- 666 [31] Schafer BW, Adany S. Buckling analysis of cold-formed steel members using CUFSM: conventional and
667 constrained finite strip methods. In: Eighteenth International Specialty Conference on Cold-Formed Steel
668 Structures, Orlando, FL, USA, 2006. p. 39-54.
- 669 [32] Buchanan C, Gardner L, Liew A. The continuous strength method for the design of circular hollow

670 sections. J Constr Steel Res. 2016;118:207-16.

671 [33] Yun X, Gardner L, Boissonnade N. The continuous strength method for the design of hot-rolled steel
672 crosssections. Eng Struc. 2018;157:179-91.

673 [34] EN 1993-1-5, Eurocode 3: Design of Steel Structures – Part 1–5: Plated structural elements. Brussels:
674 European Committee for Standardization (CEN); 2006.

675 [35] EN 1993-1-1, Eurocode 3: Design of Steel STRUCTURES – Part 1.1: General Rules and Rules for
676 Buildings. Brussels: European Committee for Standardization (CEN); 2005.

677 [36] AS/NZS 4600:2018, Cold-formed steel structures, AS/NZS 4600. Sydney, Australia and Wellington, New
678 Zealand: Australian/New Zealand Standards; 2018.

679 [37] Lan X, Chen J, Chan TM, Young B. The continuous strength method for the design of high strength steel
680 tubular sections in compression, Eng Struc. 2018; 162: 177-187